

Optical spectroscopy of bulk single crystals of VO_x and TiO_xTaishi Yoshida,¹ Kaoru Akimoto,¹ Asuka Yanagida,¹ Suguru Yano¹,¹ Haruka Matsumoto,¹ Takumi Iwata,¹ Ryota Yoshimura,¹ and Takuro Katsufuji^{1,2}¹Department of Physics, Waseda University, Tokyo 169-8555, Japan²Kagami Memorial Research Institute for Materials Science and Technology, Waseda University, Tokyo 169-0051, Japan

(Received 6 December 2022; accepted 19 January 2023; published 30 January 2023)

We successfully grew bulk single crystals of VO_x and TiO_x with a sodium-chloride structure by the floating-zone method, and we performed optical reflectivity measurement and pump-probe spectroscopy to clarify the electronic structure of these series of compounds and their x dependence. We found that optical spectra can be discussed on the basis of the Mott-Hubbard model, although a disorder arising from the deficiencies of V or Ti and O plays an important role in the electronic structure as well as their x dependence.

DOI: [10.1103/PhysRevMaterials.7.014412](https://doi.org/10.1103/PhysRevMaterials.7.014412)

I. INTRODUCTION

3d transition-metal oxides are typical strongly correlated electron systems, where the Coulomb repulsion between two d electrons on the same transition-metal ion (often denoted as U) is significant and dominates the electronic state of the system. Depending on the ratio of U and the transfer integral t of the d electrons, and also on the number n of d electrons per ion, the system may be an insulator (a Mott insulator) or a metal. In general, when U/t is large and n is close to an integer, the system tends to be a Mott insulator

There are various 3d transition-metal oxides that are on the border between the metallic state and the Mott-insulating state, and some of them exhibit a metal-insulator transition (Mott transition) [1]. For example, V₂O₃ [2], VO₂ [3,4], V_nO_{2n-1} with a Magneli phase [5], Ti₂O₃ [6], and Ti_nO_{2n-1} [7,8] exhibit metal-insulator transitions under temperature variation. Various ternary systems including 3d transition metals also are known to exhibit interesting behavior as strongly correlated electron systems [1], and perovskite and spinel structures are well-studied structures.

Among various 3d transition-metal oxides, transition-metal monoxides with a sodium-chloride structure can be regarded as having the simplest crystal structure. Among transition-metal monoxides, those with conduction electrons existing in the e_g states of the 3d orbitals tend to be Mott insulators because of a smaller transfer integral of the e_g state to the neighboring transition metal (T) in the edge-sharing octahedron of TO₆. Only those with d electrons in the t_{2g} states, namely, TiO and VO, can be metallic.

Physical properties of TiO_x and VO_x have been studied mainly in polycrystalline samples [9–21] and thin films [22–29]. For both compounds, x can be varied from ≈ 0.8 to ≈ 1.3 , and even at $x = 1$, there are vacancies of both V or Ti and O. The resistivity ρ of VO_x is nearly T independent for $x = 0.9$ down to a low T , but it increases with x and diverges at the lowest T for $x \geq 1.1$ [9,22,23]. The magnetic susceptibility χ of VO_x behaves in such a way that, for a small

x , χ is nearly temperature (T) independent above 100 K but increases at a low T . However, with increasing x , χ increases and begins to exhibit a Curie-Weiss T dependence [9]. On the other hand, the absolute value of ρ for TiO_x is much smaller than that for VO_x. The sign of the T derivative of ρ for TiO_x changes from positive to negative with increasing x , but ρ does not diverge at the lowest T with any x [9,18]. χ of TiO_x is almost T independent when x is small, and with increasing x , χ rather decreases at room temperature but the Curie tail at a lower T increases [18]. TiO_x is a superconductor with T_c less than 2 K [15], but T_c increases up to 7 K for thin films under strain [28] and up to 11 K for nanoparticles [20]. Theoretical studies have also been made on VO_x and TiO_x [30–32].

It should be pointed out that systematic studies on bulk single crystals of VO_x and TiO_x have not been performed extensively thus far, probably because both VO_x and TiO_x exhibit incongruent melting [9]; thus, their large single crystals are difficult to grow. Indeed, we found that a simple floating-zone method [33], in which a nominal composition of VO_x or TiO_x is melted, results in the decomposition into phases with different lattice constants, namely, different x values. Here, we found that if we apply a floating-zone method to a nominal composition of VO_x or TiO_x mixed with K₂CO₃, the decomposition is suppressed and a large single crystal with negligible inhomogeneity can be grown. In this study, we grew single crystals of VO_x and TiO_x with various x values. We then performed optical reflectivity measurement and pump-probe optical spectroscopy on these single crystals to clarify their electronic structure and x dependence.

II. EXPERIMENT

Single crystals of VO_x ($x = 1.06$ and 1.31) and TiO_x ($x = 0.93$, 1.06 , and 1.28) were grown by the floating-zone method. V and V₂O₃ for VO_x, and Ti and TiO₂ for TiO_x were mixed with K₂CO₃ at appropriate amounts (typically at a molar ratio of K : V,Ti = 1 : 10). The mixture was pressed into rods, and the rods were melted in the floating furnace in a flow of

$\text{H}_27\%/ \text{Ar}$ gas. Note that all of K_2CO_3 was evaporated during the single-crystal growth by the floating-zone method. The powder x-ray diffraction of the ground crystals was measured to obtain the lattice constant, and Laue diffraction was measured to determine the crystal axes. The results of the x-ray diffraction are summarized in the Appendix. x was estimated on the basis of the relationship between the lattice constant and the value of x for VO_x and TiO_x previously reported, and by thermogravimetric analysis (TGA), which showed that the results are almost consistent with each other. We use the value obtained by TGA in this paper. The resistivity of the crystals was measured by a four-probe technique. Magnetic susceptibility was measured using a SQUID magnetometer at an applied magnetic field of 0.1 T.

For optical measurements, the crystals were cut and polished with Al_2O_3 powder. All the optical measurements were performed at room temperature. Optical reflectivity was measured using a FTIR spectrometer between 0.1 and 0.8 eV and by a grating spectrometer between 0.7 and 5 eV. Pump-probe optical spectroscopy was performed using a Ti:sapphire regenerative amplified laser (a pulse width of 130 fs, a repetition rate of 1 kHz, and a wavelength of 795 nm) [34]. A pump pulse with a power density of 18 or 24 mJ/cm^2 was applied to the crystals. A probe pulse was generated by focusing a laser pulse from the same laser as used for the pump pulse into circulating water in the optical cell, where the frequency of the light was broadened in frequency between $\hbar\omega = 0.8$ and 3.0 eV by the self-phase modulation. The light pulse thus generated was focused onto the sample surface and the reflected light was monochromated by a monochromator and was detected using a Si photodiode. The time delay between the pump pulse and the probe pulse was controlled by controlling the difference in optical path length by an optical stage.

III. RESULTS

Figure 1 shows the dc resistivity ρ and the magnetic susceptibility χ as functions of temperature T for VO_x and TiO_x . As can be seen, the T derivative of ρ ($d\rho/dT$) is negative for VO_x and the one with $x = 1.31$ is more insulating than that with $x = 1.06$. Such behavior is consistent with the results of the polycrystalline forms [9] and thin films [22,23] of VO_x . On the other hand, ρ of TiO_x is lower than that of VO_x , and the sign of $d\rho/dT$ changes with x from positive ($x < 1$) to negative ($x > 1$) [9,18]. The absolute value of ρ for $x = 1.06$ is much smaller than those for other x values. According to a previous study, monoclinic TiO_x exhibits a lower resistivity than cubic TiO_x [9] probably owing to the ordering of Ti or O defects [14,19]. We speculate that this also affects the smaller values of ρ for our single crystal with $x = 1.06$. Note that our TiO_x single crystals have a slight monoclinic distortion, as seen in the splitting of the x-ray diffraction peak shown in the Appendix [Fig. 10(b)]. The magnetic susceptibilities of TiO_x for $0.93 \leq x \leq 1.28$ are similar to each other and a clear x dependence is barely observed.

Figure 2(a) shows the optical reflectivity spectra [$R(\omega)$] for VO_x with $x = 1.06$ and 1.31. R decreases with increasing $\hbar\omega$, reaching the minimum at ≈ 3.5 eV, and it increases with increasing $\hbar\omega$ at energies higher than 3.5 eV. With increasing x , reflectivity below 2 eV decreases whereas that above 2 eV

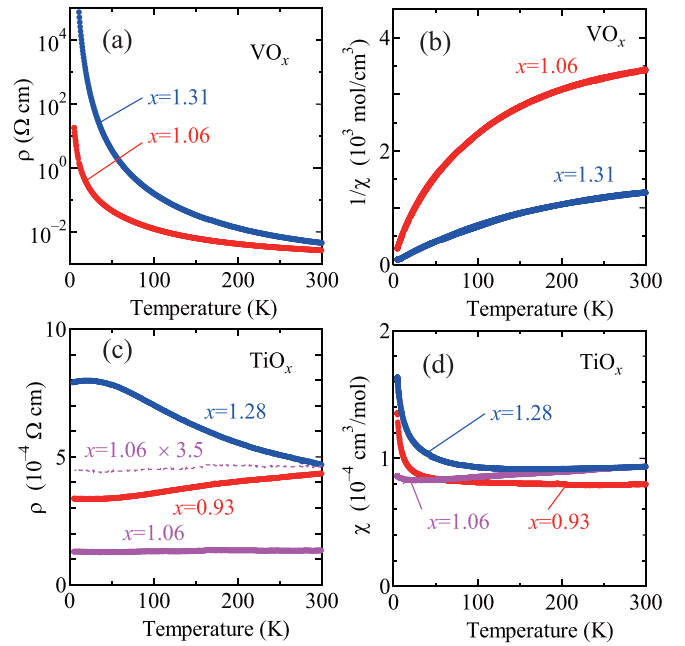


FIG. 1. (a), (c) Resistivity and (b) inverse magnetic susceptibility and (d) magnetic susceptibility for (a), (b) VO_x and (c), (d) TiO_x .

increases. Figure 2(b) shows the optical conductivity spectra [$\sigma(\omega)$] for VO_x crystals derived from their $R(\omega)$ spectra by the Kramers-Kronig transformation. A broad structure from 0 to 3 eV, which is followed by an increase above 3 eV, is observed for both x . The increase in $\sigma(\omega)$ above 3 eV can be attributed to the so-called charge-transfer (CT) excitation; that is, the excitation from the oxygen 2p level to the upper Hubbard band of the V 3d orbital, which can be commonly observed in various vanadium oxides for a similar $\hbar\omega$ range, as discussed below.

On the other hand, the broad structure below 3 eV is unique in the present series of compounds. For example, for VO_2 , a typical Drude spectrum in $\sigma(\omega)$, which increases with decreasing $\hbar\omega$ to 0 eV, is observed at high temperatures in the metallic phase, whereas a gap opens below $\hbar\omega \approx 0.5$ eV at low temperatures in the insulating phase [35]. For V_2O_3 , a nearly $\hbar\omega$ -independent spectrum with small structures is observed in $\sigma(\omega)$ at high temperatures in the metallic phase, whereas a gap of ≈ 0.5 eV opens at low temperatures in the

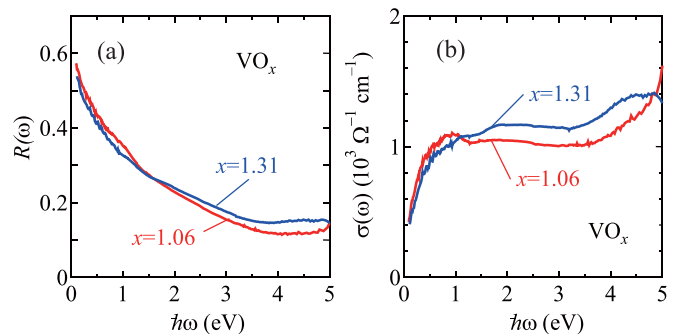


FIG. 2. (a) Reflectivity and (b) optical conductivity spectra for VO_x with $x = 1.06$ and 1.31.

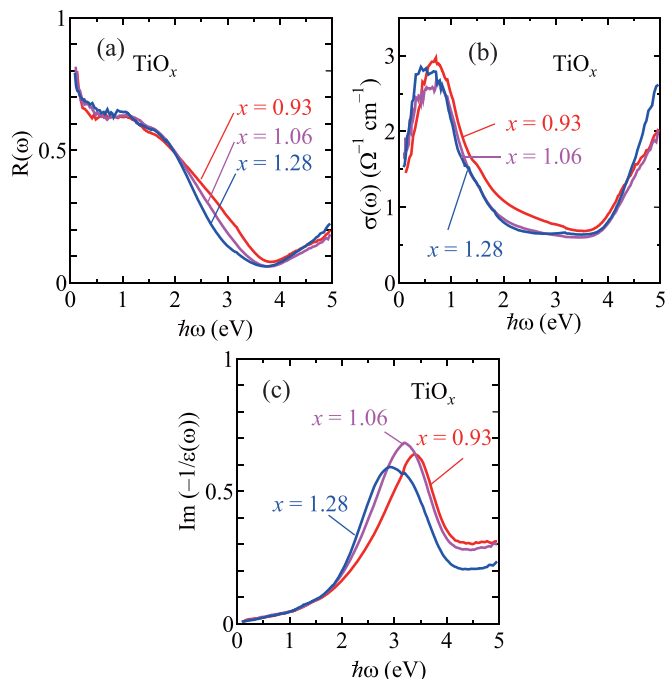


FIG. 3. (a) Reflectivity, (b) optical conductivity, and (c) loss function spectra for TiO_x with $x = 0.93, 1.06,$ and 1.28 .

insulating phase [35]. Compared with these spectra, those for VO_x are between the spectra for the metallic and insulating phases, where $\sigma(\omega)$ decreases with decreasing $\hbar\omega$ at energies below 0.5 eV, similarly to the spectra for a typical insulating phase, although $\sigma(\omega)$ remains a finite value at $\hbar\omega = 0$, similarly to the spectra for the metallic phase. As for the

x dependence of the $\sigma(\omega)$ spectra, the spectrum at energies below 1 eV decreases, whereas that at energies above 1 eV increases with increasing x . This is qualitatively consistent with a more insulating character in the dc resistivity for a larger x .

The $R(\omega)$ spectra for TiO_x with $x = 0.93, 1.06,$ and 1.28 are shown in Fig. 3(a). $R(\omega)$ is nearly $\hbar\omega$ -independent up to ≈ 1.5 eV, then it decreases with increasing $\hbar\omega$, reaches a minimum at ≈ 4 eV, after which it begins to increase. With increasing x , the $R(\omega)$ spectrum between 2 and 4 eV shifts to a lower energy. Figure 3(b) shows the $\sigma(\omega)$ spectra for TiO_x derived from their $R(\omega)$ spectra. Compared with those for VO_x , a clear increase in $\sigma(\omega)$ with decreasing $\hbar\omega$ below 2 eV is observed in the spectra for TiO_x . However, this increase is not due to a Drude spectrum, a typical spectrum for a metallic state, but $\sigma(\omega)$ decreases with decreasing $\hbar\omega$ below 0.5 eV. Note that the values of $\sigma(\omega)$ at the limit of $\hbar\omega = 0$ eV, i.e., $\approx 4 \times 10^2 \Omega^{-1} \text{cm}^{-1}$ for VO_x and $\approx 2 \times 10^3 \Omega^{-1} \text{cm}^{-1}$ for TiO_x , are almost consistent with the dc resistivity at 300 K for these series of compounds, except for TiO_x with $x = 1.06$.

The x dependence of the $\sigma(\omega)$ spectra for TiO_x shown in Fig. 3(b) does not appear systematic. Indeed, a systematic x dependence of the optical spectra for TiO_x is more clearly seen in the loss function, $\text{Im}[-1/\epsilon(\omega)]$, as shown in Fig. 3(c). Note that the loss function corresponds to the longitudinal excitation, whereas $\sigma(\omega)$ corresponds to the transverse excitation, and the $R(\omega)$ spectra are dominated both by $\sigma(\omega)$ and $\text{Im}[-1/\epsilon(\omega)]$. As can be seen in Fig. 3(c), the peak in the loss function at $\hbar\omega \approx 3$ eV shifts to lower values with increasing x . Since the peak frequency of the loss function corresponds to the spectral weight of $\sigma(\omega)$, the present experimental result means that the spectral weight of $\sigma(\omega)$ at energies below 3 eV decreases with increasing x .

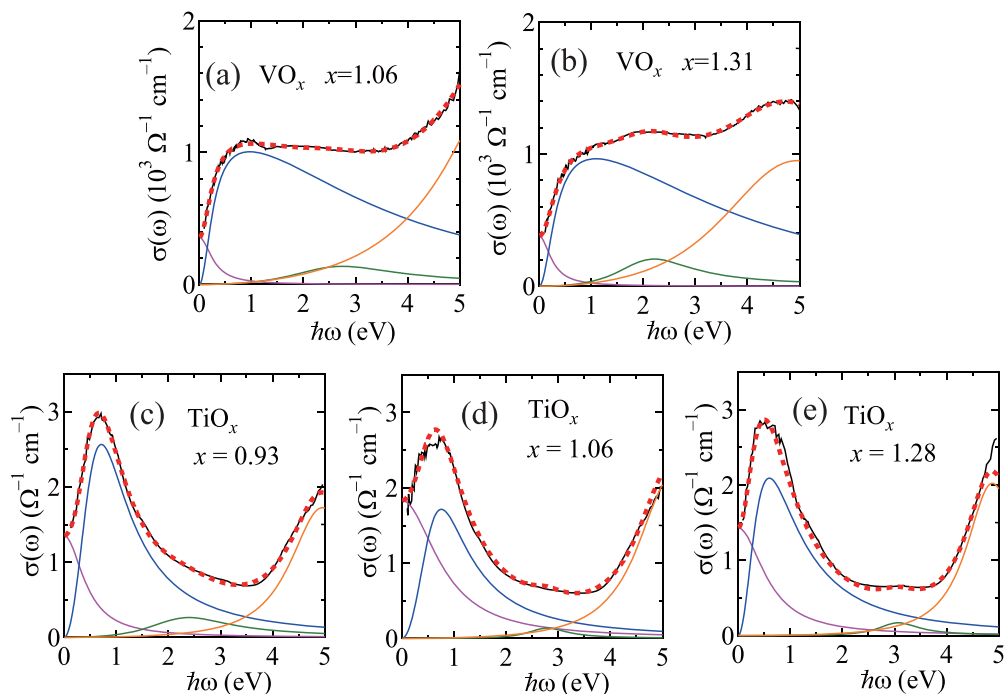


FIG. 4. Result of fitting of the optical conductivity spectra to Eqs. (1) and (2) (dashed line) and each component (thin solid lines) for VO_x with (a) $x = 1.06$ and (b) 1.31 , and for TiO_x with (c) $x = 0.93$, (d) 1.06 , and (e) 1.28 .

To quantitatively understand these spectra, we fit the optical conductivity spectra of both VO_x and TiO_x using one Drude term and three Lorentz functions:

$$\epsilon(\omega) = \epsilon_\infty - \frac{\omega_p^2}{\omega^2 + i\omega\gamma_p} + \sum_{i=1}^3 \frac{S_i\omega_i^2}{\omega_i^2 - \omega^2 - i\omega\gamma_i}, \quad (1)$$

$$\sigma(\omega) = \text{Im}\{\omega\epsilon(\omega)\}, \quad (2)$$

where $\epsilon(\omega)$ is the (dimensionless) complex dielectric function. The fitting results are shown by dashed lines in Figs. 4 and the parameters obtained by the fitting are summarized in the Appendix. For the three Lorentz functions, the one with ω_3 ($\hbar\omega_3 > 4$ eV) corresponds to the CT excitation. Such an excitation exists at ≈ 3.5 eV for LaVO_3 [36], ≈ 3 eV for V_2O_3 [35], ≈ 4 eV for LaTiO_3 [36], and ≈ 4 eV for Ti_2O_3 [37], as the onset of the peak in the optical conductivity spectrum. Thus, the onset of the peak with ω_3 at ≈ 4 eV for TiO_x and ≈ 3.5 eV for VO_x in the present study is consistent with the tendency of the vanadate and titanates in the previous studies. The remaining two Lorentz functions ($\hbar\omega_2 = 2\text{--}3$ eV and $\hbar\omega_1 \approx 1$ eV) are most likely assigned to the Mott excitation and in-gap excitation. In strongly correlated electron systems, for example, in those described by the Hubbard model with the onsite Coulomb repulsion U between two electrons on the same site and the transfer integral t of the electron, the $\sigma(\omega)$ spectrum is composed of a Mott excitation at $\approx U$, an in-gap excitation at $\approx U/2$, and a Drude spectrum at $\hbar\omega = 0$ [38]. On the basis of this picture, the Lorentz function with ω_2 can be assigned to the Mott excitation and that with ω_1 to the in-gap excitation.

One of the striking features in the fitting results of the $\sigma(\omega)$ spectra for VO_x and TiO_x is the presence of a large portion of the spectral weight for the in-gap excitation (ω_1) and a relatively small portion of the Drude spectrum and the Mott excitation (ω_2). Theoretically and experimentally, with decreasing U/t or varying the number of carriers per site from unity, the spectral weight of the Mott excitation decreases whereas that of the Drude spectrum and in-gap excitation increases [1,38]. For vanadium oxides, the Drude excitation and possibly the in-gap excitation have a much larger spectral weight than the Mott excitation for VO_2 , meaning a relatively small U/t , whereas all the Drude, in-gap, and Mott excitations have comparable spectral weight for V_2O_3 , meaning a larger U/t [35]. For the present compounds, although the spectral weight of the Mott excitation is relatively small, the in-gap excitation is dominant and the Drude weight is much smaller than that of the in-gap excitation. Such an anomalous ratio in the spectral weight suggests that disorder in VO_x and TiO_x arising from the deficiencies of V, Ti, and O ions causes the transfer of the spectral weight from the Drude component to the in-gap component.

As seen in Fig. 4, the $\sigma(\omega)$ spectra for both series of compounds, particularly for VO_x , are relatively structureless and the decomposition of the spectra may include some uncertainty. To further identify each structure, we performed pump-probe measurements on these series of compounds. Figures 5(a) and 5(b) show the photoinduced changes in the reflectivity spectra $\Delta R/R$ for VO_x with $x = 1.06$ and 1.31 at 0.3 and 2 ps after the irradiation of a pump pulse. As can be seen, $\Delta R/R$ is positive at lower $\hbar\omega$ and negative at higher $\hbar\omega$,

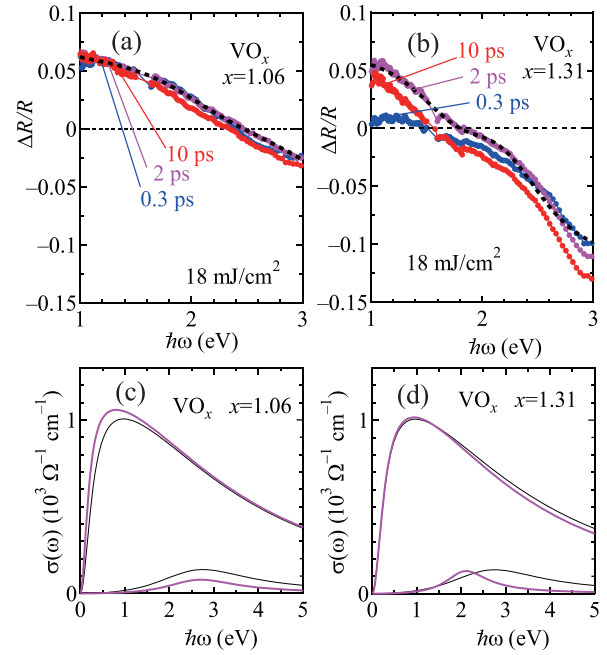


FIG. 5. (a), (b) Photoinduced change in the reflectivity spectra $\Delta R/R$ for VO_x with (a) $x = 1.06$ and (b) 1.31 at 0.3, 2, and 10 ps after a pump pulse is applied. Dashed lines are the result of the fitting for the data at 2 ps. (c), (d) Lorentz functions with $\hbar\omega_1 \approx 1$ eV and $\hbar\omega_2 \approx 2.5$ eV before (thin black lines) and after (thick magenta lines) the irradiation of a pump pulse for (c) $x = 1.06$ and (d) 1.31.

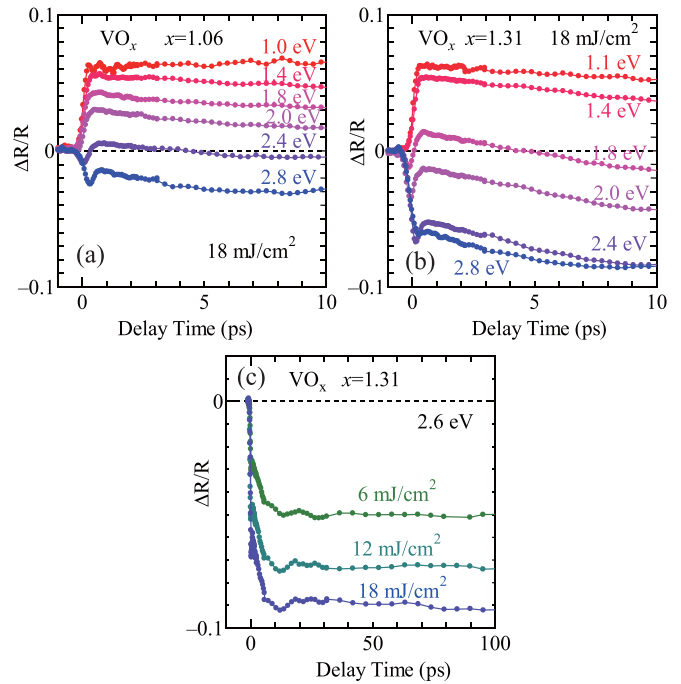


FIG. 6. Time dependence of the photoinduced change in the reflectivity $\Delta R/R$ for VO_x (a) with $x = 1.06$ and (b) $x = 1.31$ at various values of $\hbar\omega$ of the probe pulse up to $t = 10$ ps, and (c) with $x = 1.31$ at $\hbar\omega = 2.6$ eV with various power densities of the probe pulse up to $t = 100$ ps.

and the value of $\hbar\omega$ at which $\Delta R/R$ becomes zero is 2.5 eV at 2 ps for $x = 1.06$, but it decreases to 1.7 eV for $x = 1.31$.

Figures 6(a) and 6(b) show the time (t) dependence of the photoinduced change in the reflectivity $\Delta R/R$ for VO_x with $x = 1.06$ and 1.31 at various $\hbar\omega$ values up to 10 ps. For both x values at any $\hbar\omega$, $\Delta R/R$ sharply changes near $t = 0$ ps and then barely changes. We found that $\Delta R/R$ at the same $\hbar\omega$ shifts to lower values for $x = 1.31$ compared with $x = 1.06$, consistent with the $\Delta R/R$ spectra shown in Figs. 5(a) and 5(b). A slight decrease in $\Delta R/R$ with t up to 10 ps is likely caused by the oscillation of $\Delta R/R$ with t associated with shockwaves, whose propagation speed is dominated by the sound velocity of the compound. This is more clearly seen in Fig. 6(c), where the t dependence of the photoinduced $\Delta R/R$ at $\hbar\omega = 2.6$ eV for $x = 1.31$ is plotted up to 100 ps. In the same figure, the t dependence of $\Delta R/R$ is plotted at various power densities of the pump pulse p . As can be seen, the absolute value of $\Delta R/R$ increases with increasing p , but the increase in $\Delta R/R$ is less than the linear dependence of p , meaning a saturation behavior.

To analyze the photoinduced $\Delta R/R$ spectra shown in Fig. 5, we calculate the change in the reflectivity spectrum using the following formula of reflectivity:

$$R(\omega) = \left| \frac{\sqrt{\epsilon(\omega)} - 1}{\sqrt{\epsilon(\omega)} + 1} \right|^2, \quad (3)$$

before and after the change in the parameters of some of the Lorentz functions obtained by the fitting of the experimentally obtained $\sigma(\omega)$ spectrum. We found that the photoinduced $\Delta R/R$ spectra obtained in the experiment can be reproduced by changing the parameters of only the first (in-gap excitation) and second (Mott excitation) Lorentz functions. The fitting results of the $\Delta R/R$ spectra at 2 ps are shown by dashed lines in Figs. 5(a) and 5(b). The changes in the two Lorentz functions of the $\sigma(\omega)$ spectrum are shown in Figs. 5(c) and 5(d) and the parameters are summarized in the

Appendix. As can be seen, the spectral weight for the second Lorentz function is reduced whereas that for the first one is increased by photoirradiation. In many strongly correlated electrons systems, the Mott-excitation spectrum is suppressed whereas the Drude and in-gap excitations are enhanced by photoirradiation [39,40]; thus, the present experimental results are consistent with the assignment of the first and second Lorentz functions to the in-gap and Mott excitations, respectively.

The x dependence of the spectra for VO_x can be described as follows: For the $\sigma(\omega)$ spectrum, the spectral weight of the Mott excitation increases with x . With photoirradiation, however, the reduction in the spectral weight of the Mott excitation becomes larger with increasing x , resulting in the shift of $\hbar\omega$ at which the photoinduced $\Delta R/R$ becomes zero to a lower value. In general, the Mott excitation is enhanced when the system becomes more insulating (owing to the increase in U/t , for example). The photoirradiation in such a system roughly corresponds to carrier doping, and it is reasonable to consider that if the system is closer to the Mott insulating state, the change in the spectrum with carrier doping becomes more significant. These are consistent with the present experimental results.

We also performed the pump-probe measurements of TiO_x and the results are shown in Figs. 7(a)–7(c). The $\Delta R/R$ spectra exhibit a dip at $\hbar\omega \approx 2$ eV, and the depth of the dip increases and the position of the dip shifts to a higher $\hbar\omega$ with increasing x .

The time (t) dependence of photoinduced $\Delta R/R$ for TiO_x up to 10 ps is shown in Figs. 8(a)–8(c). Unlike in the case of VO_x , there is a clear t dependence of $\Delta R/R$, particularly at $\hbar\omega$ above 2 eV, in such a way that $\Delta R/R$ becomes negative immediately after $t = 0$ (application of a pump pulse). Then, its absolute value decreases to zero within 1 ps, after which $\Delta R/R$ becomes negative again for ≈ 5 ps. Such t dependence manifests itself in the $\Delta R/R$ spectra shown in Figs. 7(a)–7(c), where only the spectrum at 1 ps shifts to higher values above 2 eV. The t dependence of $\Delta R/R$ in this range is dominated

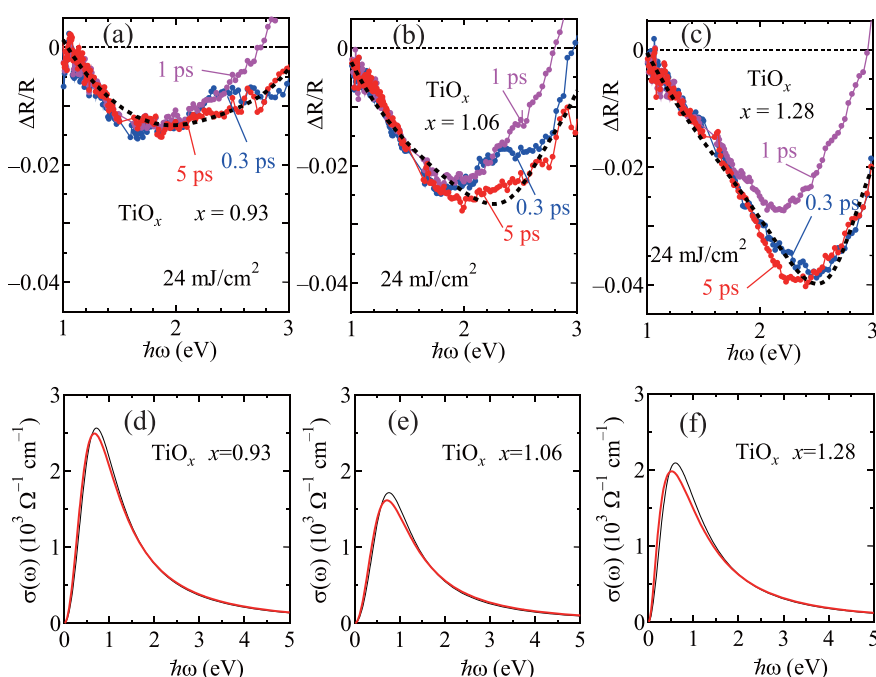


FIG. 7. Photoinduced changes in the reflectivity spectra $\Delta R/R$ for TiO_x with (a) $x = 0.93$, (b) 1.06, and (c) 1.28 at 0.3, 1, and 5 ps after a pump pulse is applied. Dashed lines are the results of the fitting of the data at 1 ps. Lorentz functions with $\hbar\omega_1 \approx 0.6$ eV before (thin black lines) and after (thick red lines) the irradiation of a pump pulse for (d) $x = 0.93$, (e) 1.06, and (f) 1.28.

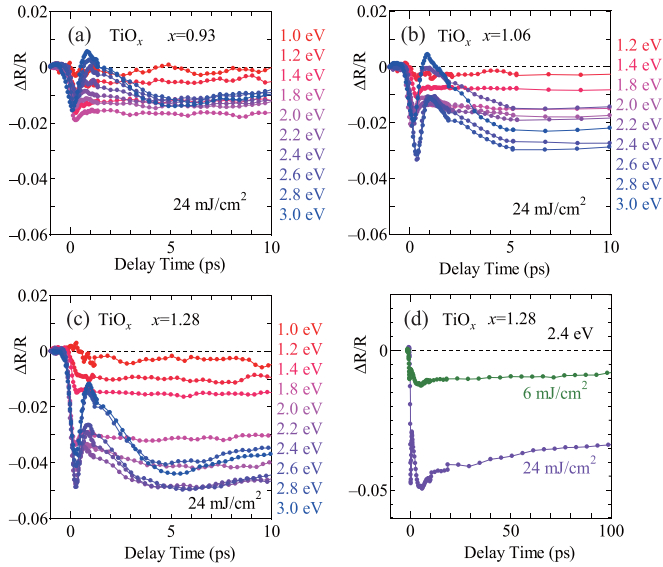


FIG. 8. Time dependence of the photoinduced change in the reflectivity $\Delta R/R$ for TiO_x (a) with $x = 0.93$, (b) $x = 1.06$, and (c) $x = 1.28$ at various $\hbar\omega$ values of the probe pulse up to 10 ps, and (d) with $x = 1.28$ at $\hbar\omega = 2.4$ eV with two different power densities of the probe pulse up to $t = 100$ ps.

by the excitation of electrons, which occurs much shorter than 1 ps, and the subsequent transfer of energy from electrons to phonons for several picoseconds. The difference in the t dependence of photoinduced change in the optical spectrum between VO_x and TiO_x may be related to the smaller correlation of electrons in TiO_x , which makes the energy transfer from the electronic excitation to phononic excitations more difficult. Figure 8(d) shows the photoinduced $\Delta R/R$ for TiO_x with $x = 1.28$ at $\hbar\omega = 2.4$ eV with $p = 6$ and 24 J/cm² up to 100 ps. Similarly to VO_x shown in Fig. 6(c), $\Delta R/R$ persists up to 100 ps, indicating that it is dominated by the increase in the lattice temperature. However, unlike the case of VO_x , the absolute value of $\Delta R/R$ increases almost linearly with p with no sign of saturation.

We analyzed the $\Delta R/R$ spectra for TiO_x shown in Figs. 7(a)–7(c) similarly to those for VO_x . In the case of TiO_x , we found that changes in the parameters of only the first Lorentz function are sufficient to reproduce the $\Delta R/R$ spectra, as shown by dashed lines in Figs. 7(a)–7(c). The results of the fitting indicate that the width γ_1 increases and the peak position ω_1 shifts to lower frequencies upon the photoirradiation of TiO_x , as shown in Figs. 7(d)–7(f) and the Appendix. Qualitatively, these changes correspond to that occurring when the temperature increases for the system on the border between the insulating and metallic states. Similar photoinduced changes were observed in other strongly correlated electron systems in a nearly metallic state [41].

We found that the x dependence of the photoinduced $\Delta R/R$ is more clearly observed in the change in loss function caused by photoirradiation, as shown in Fig. 9, where the change obtained by the fitting is plotted. Both the decrease in ω_1 and the increase in γ_1 contribute to such a change in loss function between 1 and 3 eV and the change in the reflectivity. The amount of change in loss function induced by photoirradiation

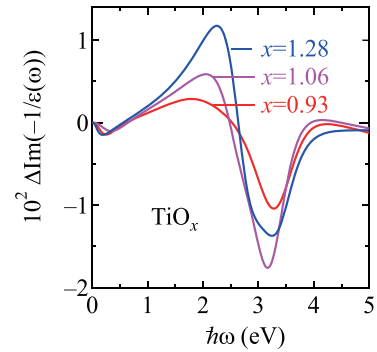


FIG. 9. Changes in the loss function $\text{Im}[-1/\epsilon(\omega)]$ with the irradiation of a pump pulse for TiO_x with $x = 0.93$, 1.06, and 1.28 obtained by the fitting.

increases with x . This can be interpreted, similarly to VO_x , that the effect of the photoinduced change, which is equivalent to carrier doping, becomes more significant when the system becomes closer to a Mott insulator.

IV. DISCUSSION

Let us first compare VO_x and TiO_x with other vanadates or titanates in terms of the electronic structure. As discussed above, VO_2 and V_2O_3 exhibit a metal-insulator transition with T , and in the metallic phase, the $\sigma(\omega)$ spectrum is dominated by a Drude excitation in VO_2 , whereas Drude, in-gap, and Mott excitations with comparable spectral weights exist in V_2O_3 [35]. In the case of Ti_2O_3 , a large peak centered at ≈ 1 eV with large spectral weight exists in $\sigma(\omega)$ [6,37], but it arises from the excitation within the Ti dimers, peculiar to the corundum structure. The vanadates and titanates with a perovskite structure are Mott insulators with integer filling, where a gap structure appears in $\sigma(\omega)$, but they can be metallic with hole doping, where a Drude component becomes dominant in $\sigma(\omega)$ [42,43]. Compared with their spectra, the $\sigma(\omega)$ spectra of VO_x and TiO_x have a unique characteristic, where, even though the compounds are metallic or close to metallic, the spectral weight of the Drude component is smaller than that of the in-gap component, which can be fit by a Lorentz function. We speculate that the deficiencies of Vi or Ti and O, which exist even in a seemingly stoichiometric compound of $x = 1$, act as disorders and change the Drude component to the in-gap component.

A comparison between VO_x and TiO_x indicates that a larger spectral weight exists in the region of $\hbar\omega < 2$ eV for TiO_x , suggesting a more metallic characteristic of TiO_x than of VO_x . This is consistent with the lower dc resistivity of TiO_x than of VO_x . Such a difference might be due to the difference in the number of d electrons (two for TiO_x and three for VO_x), which results in the difference in the onsite Coulomb repulsion U (larger for VO_x).

Regarding the x dependence, with increasing x , a smaller spectral weight exists in the Drude and in-gap components of the $\sigma(\omega)$ spectra for both VO_x and TiO_x . Furthermore, a photoinduced change in reflectivity increases with x for both VO_x and TiO_x . These results indicate that both VO_x and TiO_x become more insulating with increasing x . Note that, if these

are conventional Mott systems, they are insulating when $x = 1$ and become conducting when x is less or larger than one. The present experimental result on the electronic structure indicates that there is no such anomaly at $x = 1$, but the system monotonically changes from a more conducting state when $x < 1$ or $x \approx 1$ to a less conducting state when $x > 1$ both in VO_x and TiO_x . This also suggests the role of vacancies as disorder, which cancel out such a peculiar x dependence of conventional Mott systems.

Finally, let us discuss the origin of this x dependence. For TiO_x , with increasing x , the number of d electron decreases; thus, the magnitude of onsite Coulomb repulsion U also decreases. Simultaneously, the lattice constant becomes smaller [9]; thus, the transfer integral t becomes larger. Accordingly, there is no reason that TiO_x becomes more insulating with increasing x in terms of the Mott-Hubbard model. Again, we speculate that the deficiencies of ions as disorders play important roles in this behavior. In both TiO_x and VO_x , the number of the deficient cations, Ti or V, increases with x ; thus, we speculate that disorders arising from the deficiencies of Ti or V cause the reduction in effective transfer integral and a more insulating characteristic for not only TiO_x but also VO_x .

V. SUMMARY

Single crystals of VO_x and TiO_x with a sodium-chloride structure were grown by the floating-zone method, in which the decomposition during the crystal growth was suppressed by mixing K_2CO_3 with the starting material. The optical reflectivity of these single crystals was measured and it was found that the optical conductivity spectra for both VO_x and TiO_x can be fit by the sum of a Drude spectrum and three Lorentz functions, possibly corresponding to an in-gap state, Mott-gap excitation, and CT excitation. We found a larger spectral weight of the in-gap state than of the Drude component, which is possibly caused by the disorders arising from the deficiencies of cations (V or Ti) and O, which transfers the Drude component into the in-gap component. We also found that, with increasing x , the spectral weight of the Mott-excitation peak increases for VO_x whereas the sum of the spectral weight of the Drude and in-gap components decreases for TiO_x . These results are consistent with the result of the dc resistivity, which exhibits a more insulating behavior with increasing x for both VO_x and TiO_x .

Pump-probe optical spectroscopy was also performed on these single crystals, which showed that the photoinduced change in reflectivity for VO_x can be attributed to the suppression of the Mott-excitation peak and the evolution of the in-gap state, whereas that for TiO_x can be explained by the increase in the width and the shift to lower frequencies of the peak for the in-gap state. For both compounds, the photoinduced changes become more significant with increasing x . Assuming that the photoinduced changes are equivalent to the changes associated with carrier doping, the present results mean that the changes in the optical spectra with doping become more significant when the system becomes more insulating. This is consistent with the idea that the two present series of compounds are both Mott-Hubbard systems. Nevertheless, anomalies as expected for Mott-Hubbard systems are barely observed upon integer filling, $x = 1$, for either

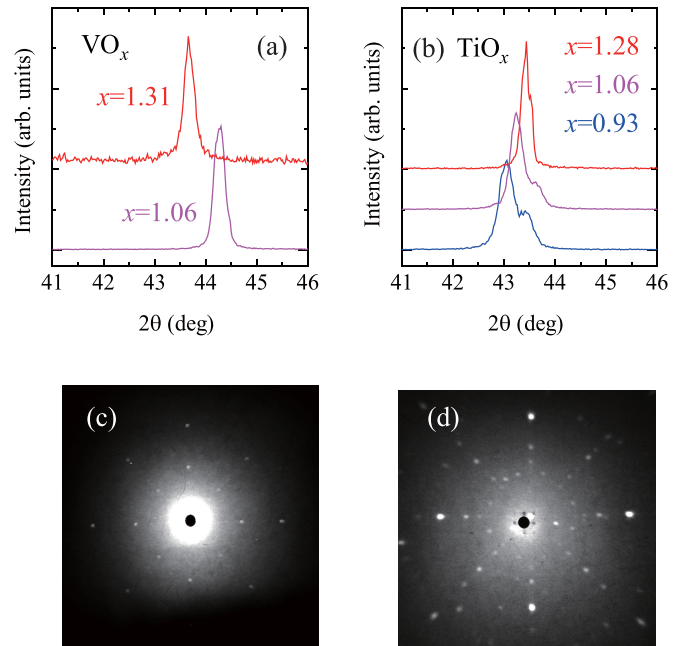


FIG. 10. Power x-ray patterns around 200 peak for (a) VO_x and (b) TiO_x . Laue diffraction patterns of the (001) plane for (c) VO_x and (d) TiO_x .

series of compounds, indicating that the electronic states are significantly affected by the disorders arising from Ti, V and O deficiencies.

ACKNOWLEDGMENTS

We thank T. Mizokawa for enlightening discussions. This work was supported by JSPS KAKENHI Grants No. 22H01172 and No. 22H04484W and Waseda University Grant for Special Research Projects (Project No. 2020R-032).

APPENDIX

The powder x-ray diffraction and Laue diffraction patterns are shown in Fig. 10.

Nominal x values (x for VO_x or TiO_x for the starting materials), the lattice constants, and the x values estimated from the lattice constants and from TGA are shown in Table I.

The parameters obtained by the fitting of the optical spectra are summarized in Table II for VO_x and in Table III for TiO_x .

TABLE I. Nominal x values, the lattice constants, and the x values estimated from the x-ray and TGA for VO_x and TiO_x .

Nominal x	Lattice constant (Å)	x from x-ray	x from TGA
VO_x			
1.0	4.090	1.05	1.06
1.3	4.140	1.30	1.31
TiO_x			
0.9	4.194	0.80	0.93
1.0	4.178	1.10	1.06
1.2	4.167	1.30	1.28

TABLE II. Parameters obtained by the fitting of the $\sigma(\omega)$ spectra (odd rows) and changes in some parameters obtained from the photoinduced $\Delta R/R$ spectra (even rows) for VO_x .

x	ω_p (eV)	γ_0 (eV)	ω_1 (eV)	γ_1 (eV)	S_1	ω_2 (eV)	γ_2 (eV)	S_2	ω_3 (eV)	γ_3 (eV)	S_3
1.06	0.869	0.284	0.970	3.716	29.55	2.751	2.514	0.340	6.715	3.949	1.448
			-0.163	-0.055	1.08	-0.042	-0.613	-0.192			
1.31	0.860	0.261	1.090	3.949	23.86	2.205	1.786	0.563	4.961	3.769	1.084
			-0.149	-0.481	-1.80	-0.091	-0.644	-0.335			

TABLE III. Parameters obtained by the fitting of the $\sigma(\omega)$ spectra (odd rows) and changes in some parameters obtained from the photoinduced $\Delta R/R$ spectra (even rows) for TiO_x .

x	ω_p (eV)	γ_0 (eV)	ω_1 (eV)	γ_1 (eV)	S_1	ω_2 (eV)	γ_2 (eV)	S_2	ω_3 (eV)	γ_3 (eV)	S_3
0.93	2.120	0.447	0.714	1.152	43.04	2.390	1.923	0.662	4.956	1.555	0.812
			-0.045	0.051	0.67						
1.06	3.330	0.814	0.757	1.14	26.13	2.786	0.917	0.120	5.182	1.629	0.968
			-0.043	0.098	0.52						
1.28	2.538	0.600	0.600	1.192	51.46	3.074	0.952	0.128	4.878	1.237	0.782
			-0.082	0.074	0.31						

- [1] M. Imada, A. Fujimori, and Y. Tokura, Metal-insulator transitions, *Rev. Mod. Phys.* **70**, 1039 (1998).
- [2] D. B. McWhan, A. Menth, J. P. Remeika, W. F. Brinkman, and T. M. Rice, Metal-insulator transitions in pure and doped V_2O_3 , *Phys. Rev. B* **7**, 1920 (1973).
- [3] F. J. Morin, Oxides Which Show a Metal-to-Insulator Transition at the Néel Temperature, *Phys. Rev. Lett.* **3**, 34 (1959).
- [4] T. C. Koethe, Z. Hu, M. W. Haverkort, C. Schüssler-Langeheine, F. Venturini, N. B. Brookes, O. Tjernberg, W. Reichelt, H. H. Hsieh, H.-J. Lin, C. T. Chen, and L. H. Tjeng, Transfer of Spectral Weight and Symmetry Across the Metal-Insulator Transition in VO_2 , *Phys. Rev. Lett.* **97**, 116402 (2006).
- [5] S. Kachi, K. Kosuge, and H. Okinaka, Metal-insulator transition in $\text{V}_n\text{O}_{2n-1}$, *J. Solid State Chem.* **6**, 258 (1973).
- [6] M. Uchida, J. Fujioka, Y. Onose, and Y. Tokura, Charge Dynamics in Thermally and Doping Induced Insulator-Metal Transitions of $(\text{Ti}_{1-x}\text{V}_x)_2\text{O}_3$, *Phys. Rev. Lett.* **101**, 066406 (2008).
- [7] S. Lakkis, C. Schlenker, B. K. Chakraverty, R. Buder, and M. Marezio, Metal-insulator transitions in Ti_4O_7 single crystals: Crystal characterization, specific heat, and electron paramagnetic resonance, *Phys. Rev. B* **14**, 1429 (1976).
- [8] M. Onoda, Phase transitions of Ti_3O_5 , *J. Solid State Chem.* **136**, 67 (1998).
- [9] M. D. Banus, T. B. Reed, and A. J. Strauss, Electrical and magnetic properties of TiO and VO , *Phys. Rev. B* **5**, 2775 (1972).
- [10] J. B. Goodenough, Influence of atomic vacancies on the properties of transition-metal oxides. I. TiO_x and VO_x , *Phys. Rev. B* **5**, 2764 (1972).
- [11] S. Takagi, K. Yoshio, H. Yasuoka, T. Ohtani, K. Kosuge, and S. Kachi, ^{51}V NMR studies of vanadium monoxide $\text{VO}_{1.25}$, *J. Phys. Soc. Jpn.* **49**, 521 (1980).
- [12] F. Rivadulla, J. Fernández-Rossier, M. García-Hernández, M. A. López-Quintela, J. Rivas, and J. B. Goodenough, VO : A strongly correlated metal close to a Mott-Hubbard transition, *Phys. Rev. B* **76**, 205110 (2007).
- [13] A. Gusev, D. Davydov, and A. Valeeva, Vacancy distribution in nonstoichiometric vanadium monoxide, *J. Alloys Compd.* **509**, 1364 (2011).
- [14] D. Watanabe, J. R. Castles, A. Jostsons, and A. S. Malin, The ordered structure of TiO , *Acta Crystallogr.* **23**, 307 (1967).
- [15] J. K. Hulm, C. K. Jones, R. A. Hein, and J. W. Gibson, Superconductivity in the TiO and NbO systems, *J. Low Temp. Phys.* **7**, 291 (1972).
- [16] S. R. Barman and D. D. Sarma, Electronic structure of TiO_x ($0.8 \leq x \leq 1.3$) with disordered and ordered vacancies, *Phys. Rev. B* **49**, 16141 (1994).
- [17] S. Bartkowski, M. Neumann, E. Z. Kurmaev, V. V. Fedorenko, S. N. Shamin, V. M. Cherkashenko, S. N. Nemnonov, A. Winiarski, and D. C. Rubie, Electronic structure of titanium monoxide, *Phys. Rev. B* **56**, 10656 (1997).
- [18] A. A. Valeeva, A. A. Rempel', and A. I. Gusev, Electrokinetic and magnetic properties of cubic titanium monoxide with a double-defect structure, *Dokl. Phys.* **47**, 39 (2002).
- [19] A. A. Valeeva, A. A. Rempel, and A. I. Gusev, Structure and specific heat of disordered and ordered titanium monoxide TiO_y , *J. Struct. Chem.* **44**, 235 (2003).
- [20] J. Xu, D. Wang, H. Yao, K. Bu, J. Pan, J. He, F. Xu, Z. Hong, X. Chen, and F. Huang, Nano titanium monoxide crystals and unusual superconductivity at 11 K, *Adv. Mater.* **30**, 1706240 (2018).
- [21] J. Ding, T. Ye, H. Zhang, X. Yang, H. Zeng, C. Zhang, and X. Wang, Pressure-induced structural phase transition and vacancy filling in titanium monoxide TiO up to 50 GPa, *Appl. Phys. Lett.* **115**, 101902 (2019).
- [22] A. D. Rata, V. Kataev, D. Khomskii, and T. Hibma, Giant positive magnetoresistance in metallic VO_x thin films, *Phys. Rev. B* **68**, 220403(R) (2003).

- [23] A. D. Rata, A. R. Chezan, M. W. Haverkort, H. H. Hsieh, H.-J. Lin, C. T. Chen, L. H. Tjeng, and T. Hibma, Growth and properties of strained VO_x thin films with controlled stoichiometry, *Phys. Rev. B* **69**, 075404 (2004).
- [24] A. D. Rata and T. Hibma, Strain-induced properties of epitaxial VO_x thin films, *Eur. Phys. J. B* **43**, 195 (2005).
- [25] Y. Sugizaki, H. Motoyama, K. Edamoto, and K. Ozawa, Electronic structure of the VO film grown on Ag(100): Resonant photoelectron spectroscopy study, *e-J. Surf. Sci. Nanotechnol.* **16**, 236 (2018).
- [26] H. Kaneko, M. Tanaka, K. Ozawa, and K. Edamoto, Electronic structure of the TiO thin film on Ag(100): Angle-resolved photoemission study, *Surf. Sci.* **602**, 2295 (2008).
- [27] X. Liu, C. Zhang, F. X. Hao, T. Y. Wang, Y. J. Fan, Y. W. Yin, and X. G. Li, Hydrostatic pressure effect on the transport properties in TiO superconducting thin films, *Phys. Rev. B* **96**, 104505 (2017).
- [28] C. Zhang, F. Hao, G. Gao, X. Liu, C. Ma, Y. Lin, Y. Yin, and X. Li, Enhanced superconductivity in TiO epitaxial thin films, *npj Quantum Mater.* **2**, 2 (2017).
- [29] F. Li, Y. Zou, M.-G. Han, K. Foyevtsova, H. Shin, S. Lee, C. Liu, K. Shin, S. D. Albright, R. Sutarto, F. He, B. A. Davidson, F. J. Walker, C. H. Ahn, Y. Zhu, Z. G. Cheng, I. Elfimov, G. A. Sawatzky, and K. Zou, Single-crystalline epitaxial TiO film: A metal and superconductor, similar to Ti metal, *Sci. Adv.* **7**, eabd4248 (2021).
- [30] J. K. Burdett and T. Hughbanks, NbO and TiO: A study of the structural and electronic stability of structures derived from rock salt, *J. Am. Chem. Soc.* **106**, 3101 (1984).
- [31] W. C. Mackrodt, D. S. Middlemiss, and T. G. Owens, Hybrid density functional theory study of vanadium monoxide, *Phys. Rev. B* **69**, 115119 (2004).
- [32] A. Yamasaki and T. Fujiwara, Electronic structure of the MO oxides ($M = \text{Mg, Ca, Ti, V}$) in the GW approximation, *Phys. Rev. B* **66**, 245108 (2002).
- [33] J. Billingham, P. Bell, and M. Lewis, The crystal growth of transition metal interstitial compounds by a floating zone technique, *J. Cryst. Growth* **13**, 693 (1972).
- [34] T. Saiki, T. Yoshida, K. Akimoto, D. Indo, M. Arizono, T. Okuda, and T. Katsufuji, Selection rule for the photoinduced phase transition dominated by anisotropy of strain in Ti₃O₅, *Phys. Rev. B* **105**, 075134 (2022).
- [35] M. M. Qazilbash, A. A. Schafgans, K. S. Burch, S. J. Yun, B. G. Chae, B. J. Kim, H. T. Kim, and D. N. Basov, Electrodynamic of the vanadium oxides VO₂ and V₂O₃, *Phys. Rev. B* **77**, 115121 (2008).
- [36] T. H. Aimra and Y. Tokura, Optical study of electronic structure in perovskite-type RMO₃ ($R = \text{La, Y; } M = \text{Sc, Ti, V, Cr, Mn, Fe, Co, Ni, Cu}$), *J. Phys. Soc. Jpn.* **64**, 2488 (1995).
- [37] Z. G. Li, Yangyang and Yu, L. Wang, Y. Weng, C. S. Tang, X. Yin, K. Han, H. Wu, X. Yu, L. M. Wong, D. Wan, X. R. Wang, J. Chai, Y.-W. Zhang, S. Wang, J. Wang, A. T. S. Wee, M. B. H. Breese, S. J. Pennycook, T. Venkatesan, S. Dong, et al., Electronic-reconstruction-enhanced hydrogen evolution catalysis in oxide polymorphs, *Nat. Commun.* **10**, 3149 (2019).
- [38] M. J. Rozenberg, G. Kotliar, H. Kajueter, G. A. Thomas, D. H. Rapkine, J. M. Honig, and P. Metcalf, Optical Conductivity in Mott-Hubbard Systems, *Phys. Rev. Lett.* **75**, 105 (1995).
- [39] S. Iwai and H. Okamoto, Ultrafast phase control in one-dimensional correlated electron systems, *J. Phys. Soc. Jpn.* **75**, 011007 (2006).
- [40] H. Okamoto, T. Miyagoe, K. Kobayashi, H. Uemura, H. Nishioka, H. Matsuzaki, A. Sawa, and Y. Tokura, Photoinduced transition from Mott insulator to metal in the undoped cuprates Nd₂CuO₄ and La₂CuO₄, *Phys. Rev. B* **83**, 125102 (2011).
- [41] N. Yamaguchi, A. Furuhashi, H. Nishihara, R. Murata, K. Takayama, and T. Katsufuji, Photoinduced dynamics in doped Mott insulators with polaronic conduction: Ba₂Ti₁₃O₂₂ and Ba_xTi₈O₁₆, *Phys. Rev. B* **94**, 045119 (2016).
- [42] T. Katsufuji, Y. Okimoto, and Y. Tokura, Spectral Weight Transfer of the Optical Conductivity in Doped Mott Insulators, *Phys. Rev. Lett.* **75**, 3497 (1995).
- [43] J. Fujioka, S. Miyasaka, and Y. Tokura, Doping Variation of Orbital Induced Anisotropy in the Electronic Structure of La_{1-x}Sr_xVO₃, *Phys. Rev. Lett.* **97**, 196401 (2006).